Microchimica Acta (2019) 186: 855
https://doi.org/10.1007/s00604-019-3917-4

ORIGINAL PAPER

Electrochemiluminescent immunoassay for the lung cancer biomarker CYFRA21-1 using MoO_x quantum dots

Xiangying Meng[1,2] · Xiao Chen[3] · Weihua Wu[1] · Wei Zheng[1] · Haohua Deng[1] · Luyao Xu[1] · Wei Chen[1] · Zhulai Li[1] · Huaping Peng[1]

Received: 31 May 2019 / Accepted: 11 October 2019 / Published online: 29 November 2019

Abstract

Molybdenum oxide quantum dots (MoO_x QDs) were synthesized by a one-pot method and used as a versatile probe in an electrochemiluminescent (ECL) immunoassay of the non-small cell lung cancer biomarker cytokeratin 19 fragment 21–1 (CYFRA21-1) as a model analyte. The MoO_x QDs exhibited stable and strong cathodic green ECL, with an emission peak at 535 nm, in the presence of $K_2S_2O_8$ within the potential range of −2.0 to 0 V. On exposure to CYFRA21-1, the ECL decreases because of the immunoreaction between CYFRA21-1 and its antibody which generates a barrier for electron transfer. The determination of CYFRA21-1 with favorable analytical performances was successfully realized under the optimal conditions. ECL decreases linearly in the 1 pg mL^{-1} to 350 ng mL^{-1} CYFRA21-1 concentration range, and the detection is as low as 0.3 pg mL^{-1}. Excellent recoveries from CYFRA21-1-spiked human serum indicate that the assay can be operated under physiological conditions.

Keywords Molybdenum oxide quantum dots · Electrochemiluminescent · Gold nanoparticles · Chitosan · Immunosensor · CYFRA21-1 · Peroxodisulfate · Human serum analysis

Introduction

Electrochemiluminescent (ECL) immunoassays provide an ultrasensitive and highly selective tool for detecting disease-related biomarkers. The key challenge of ECL immunosensor fabrication is the selection of a proper luminescent material [1]. Apart from traditional ones (luminol and Ru complexes), various nanomaterial-based ECL luminophores with high ECL efficiency, such as CdSe quantum dots (QDs) [2, 3], Ag_2Se@CdSe [1], CdTe [4], CeO_2 [5], ZnO/CdS [6], N-CQDs [7], and GO-g-C_3N_4 [8], have been successfully explored and used to fabricate biosensors for analytical applications. Among these nano-luminophores, QD-based ECL emitters have received much attention in view of their unique size-dependent electrochemical properties and ECL parameter tunability [9]. Although various QD-based ECL emitters, especially IIB-VIA type QDs, have been extensively designed for and applied in bioanalysis [4], innovative, stable, and highly efficient QD-based ECL luminophores for ECL sensors are still highly sought after. MoO_x QDs have been extensively studied in view of their superior electronic properties, high photostability, low toxicity, and excellent chemical stability [10–14], and have been widely employed in various fields [10, 15–17]. However, the ECL properties and related applications of MoO_x QDs remain underexplored.

We synthesized water-soluble MoO_x QDs by a one-pot environmentally friendly method and characterized them as

Xiangying Meng and Xiao Chen contributed equally to this work.

Electronic supplementary material The online version of this article (https://doi.org/10.1007/s00604-019-3917-4) contains supplementary material, which is available to authorized users.

✉ Wei Chen
chenandhu@163.com

✉ Zhulai Li
lizhulai@126.com

✉ Huaping Peng
phpfjmu@126.com

1 Department of Pharmaceutical Analysis, School of Pharmacy, Higher Educational Key Laboratory for Nano Biomedical Technology of Fujian Province, Fujian Medical University, Fuzhou 350004, China

2 Department of Medical Laboratory, Weifang Medical University, Weifang 261053, Shandong, China

3 Department of Gynecology, Fujian Cancer Hospital & Fujian Medical University Cancer Hospital, Fuzhou 350014, China

a potential ECL luminophore. The results demonstrate that these QDs exhibit excellent cathodic ECL properties in the presence of $K_2S_2O_8$ as a co-reactant, and the origin of this behavior was discussed in detail. Subsequently, MoO_x QDs were employed to fabricate a universal ECL immunosensing platform, the performance of which was evaluated for cytokeratin 19 fragment 21–1 (CYFRA21-1, biomarker used in the diagnosis of non-small cell lung cancer) as a model analyte. The platform allows rapid and sensitive CYFRA 21-1 detection and offered the benefits of good sensitivity, selectivity, wide linear range, and acceptable precision, and is therefore concluded to hold great promise for biological applications. Importantly, the insights gained in this work are expected to facilitate the construction of other high-performance ECL detection systems based on MoO_x QDs or their nanocomposites.

Materials and methods

Reagents and chemicals

MoS_2 powder was purchased from Sigma Aldrich (average diameter 90 nm; Shanghai, China) (https://www.sigmaaldrich.com/china-mainland.html), and $HAuCl_4$ was sourced from Aladdin Reagent Co., Ltd. (Shanghai, China) (https://www.aladdin-e.com/). Sodium citrate, tannic acid, H_2O_2, $K_2S_2O_8$, $NaH_2PO_4{\cdot}2H_2O$, $Na_2HPO_4{\cdot}12H_2O$, KCl, NaOH, $K_3[Fe(CN)_6]$, and $K_4[Fe(CN)_6]{\cdot}3H_2O$ were procured from Sinopharm Chemical Reagent Co., Ltd. (Shanghai, China) (https://www.reagent.com.cn/). CYFRA 21-1 and anti-CYFRA 21-1, carcino-embryonic antigen (CEA), fibronectin (FN), and α-fetoprotein (AFP) were obtained from Xiamen Wan Tai Kerry Biotechnology Co., Ltd. (Xiamen, China) (http://www.innodx.com/about/?19.html). Bovine serum albumin (BSA) was purchased from BBI Life Sciences Corporation (Shanghai, China) (https://www.sangon.com/). MoO_x QDs were synthesized by previous reported procedures with some modification [15]. Gold nanoparticles (Au NPs) were synthesized following the previously reported procedures (see details in Supporting Information) [18]. All chemicals and solvents were of analytical grade and were used without further purification.

Instruments and measurements

Transmission electron microscopy (TEM) imaging and energy-dispersive X-ray spectroscopy (EDS) elemental analysis of the MoO_x QDs were performed using a JEM-2100 instrument (JEOL, Japan). Fluorescence spectra were recorded on an Eclipse spectrofluorometer (Varian). Fourier transform infrared (FT-IR) spectra were recorded on a NicoletiS50 spectrometer (Thermo Fisher Scientific, China). Electrochemical impedance spectroscopy (EIS) measurements were conducted on a RST electrochemical work station (Suzhou Risetest Instrument Co., Ltd., China), and other electrochemical measurements were conducted on a CHI660b electrochemical workstation (Chenhua Instrument Company of Shanghai, China). ECL behavior was studied using an MPI-A ECL analyzer (Xi'An Remax Electronic Science & Technology, China) equipped with a photomultiplier tube (PMT) biased at 700 V. ECL experiments were performed in a conventional three-electrode setup comprising a modified/non-modified glassy carbon electrode (GCE, 3 mm in diameter) as a working electrode, an Ag/AgCl electrode as a reference electrode, and a Pt wire as a counter electrode.

Fabrication of the ECL immunosensor

The fabrication is illustrated in Scheme 1. The glassy carbon electrode (GCE) was successively polished with 0.3- and 0.05-μm alumina powder on fine chamois, cleaned by sequential ultrasonication in ethanol and water (3 min each), and blown dry with nitrogen. The surface of the pretreated electrode was coated with MoO_x QDs solution (8 μL, 0.035 g mL^{-1}) and dried under vacuum. Then, 5 μL of Au NP-chitosan (Au NP-CS) (5:1) was drop-cast on the electrode surface and allowed to dry under vacuum. Anti-CYFRA21-1 (5 μL, 50 μg mL^{-1}) was drop-cast on the sensing interface and left overnight at 4 °C, which was followed by 1 h incubation with BSA (5 μL, 1 wt%) to block nonspecific adsorption. Finally, the GCE was washed with deionized water to afford the label-free ECL immunosensor, which was stored at 4 °C when not in use.

To optimize ECL response conditions, we investigated factors affecting the performance of the immunosensor, e.g., the amount of immobilized MoO_x QDs, concentration of $K_2S_2O_8$, and detection solution pH (Fig. S1).

Determination of CYFRA21-1

The immunosensor was incubated with CYFRA21-1 solutions of different concentrations for 1 h at 37 °C and thoroughly washed with phosphate buffer (0.1 M, pH 7.4). Measurements were performed in PBS containing 0.1 M KCl and 0.1 M $K_2S_2O_8$ at scanning potentials range from −2.0 to 0 V, a scanning rate of 100 mV s^{-1}, and a PMT voltage of 800 V. The sensing electrode was placed into the ECL cell, and ECL signals were recorded at different CYFRA21-1 concentrations. In the presence of CYFRA21-1, signal intensity decreases because of the formation of a non-conductive immunocomplex in the immunoreaction of CYFRA21-1 with anti-CYFRA21-1, which allows the quantitation of the former.

Scheme 1 Illustration of the preparation of the ECL immunosensor platform

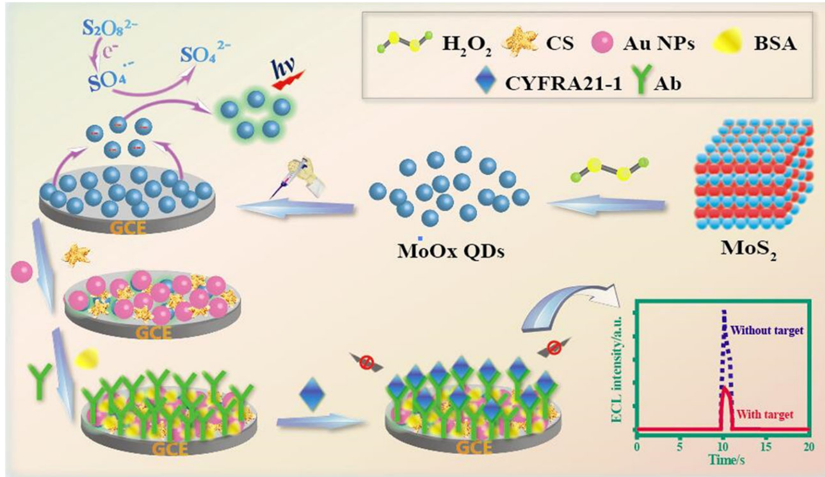

Results and discussion

Choice of materials

The MoO_x QDs were chosen because they exhibit a stable and strong cathodic ECL signal when using $K_2S_2O_8$ as the coreactant in aqueous solution of pH 7.4. Furthermore, Au NPs not only provides an effective matrix to capture a great deal of antibody, but also accelerates the electron transportation rate to enhance the ECL intensity. Combining with the excellent adhesive ability of chirosan (chit), a highly sensitive ECL immunoassay platform based on MoO_x QDs/Au NPs-chit nanocompsite film has been successfully constructed.

Characterization of the QDs

The MoO_x QDs were characterized by TEM, EDS, photoluminescence (PL), and FT-IR spectroscopy. As shown in Fig. 1a and b, the QDs are relatively uniform spherical particles (average diameter = 2–5 nm) and contain Mo and O (Fig. 1b). The FT-IR spectrum of MoO_x QDs (Fig. 1c) features three main absorption peaks at 986, 835, and 553 cm^{-1}, which are ascribed to Mo = O, doubly coordinated oxygen (Mo_2–O), and triply coordinated oxygen (Mo_3–O) stretching vibrations, respectively [19]. In addition, the fluorescence emission spectrum (λ_{ex} = 315 nm) of MoO_x QDs shows an emission maximum at 430 nm (Fig. 1d).

Performance of the assay

As already mentioned, MoO_x QDs were chosen as a novel ECL probe to develop a bioassay platform. As the inherent ECL behavior of MoO_x QDs has not been reported yet, we investigated the ECL properties of MoO_x QDs immobilized on GCE in the presence of $K_2S_2O_8$ as a co-reactant to probe the feasibility of this system. Figure 2a shows the ECL response curves of bare (curve a) and MoO_x QD-modified (curve b) GCEs recorded at a scan rate of 100 mV s^{-1} within the potential range of −2.0 to 0 V. In contrast to the case of the bare GCE, strong cathodic ECL is observed for the MoO_x QDs/GCE in the presence of externally added $K_2S_2O_8$. The intensity of the latter signal does not significantly change during 10 continuous cyclic voltammetry scans (inset of Fig. 2a), i.e., the ECL emission of the MoO_x QDs/GCE is fairly strong, stable, and hence suitable for the fabrication of ECL sensors.

The ECL spectrum of the MoO_x QDs/$S_2O_8^{2-}$ system was also investigated using a series of optical filters. As shown in Fig. 2b, the ECL emission maximum of this system is red-shifted by 105 nm relative to the PL emission maximum of MoO_x QDs at 430 nm (Fig. 1d), as has also been observed for other ECL-active nanomaterials such as methionine-stabilized Au nanoclusters [20], Si nanocrystals [21], and CdSe nanocrystals [22]. This phenomenon is ascribed to the strong effect of surface states on electrochemical and ECL processes [23]. Taken together, the above results imply that MoO_x QDs and $S_2O_8^{2-}$ can form an excellent ECL system (MoO_x QDs/$S_2O_8^{2-}$) in which QDs act as the luminophore and $S_2O_8^{2-}$ acts as the co-reactant [5, 24, 25]:

$$MoO_x\ QDs + e^- \rightarrow MoO_x^{\bullet -} \quad (1)$$

$$S_2O_8^{2-} + e^- \rightarrow SO_4^{2-} + SO_4^{\bullet -} \quad (2)$$

$$MoO_x\ QDs^{\bullet -} + SO_4^{\bullet -} \rightarrow MoO_x\ QDs^* + SO_4^{2-} \quad (3)$$

$$MoO_x\ QDs^* \rightarrow MoO_x\ QDs + h\nu \quad (4)$$

During initial potential scanning in the negative direction, MoO_x captures electrons (e^-) and is reduced to $MoO_x^{\bullet -}$, while $S_2O_8^{2-}$ is reduced to $SO_4^{\bullet -}$ and SO_4^{2-}. The reaction between $MoO_x^{\bullet -}$ and $SO_4^{\bullet -}$ affords excited MoO_x^* that emits light upon returning to the ground state.

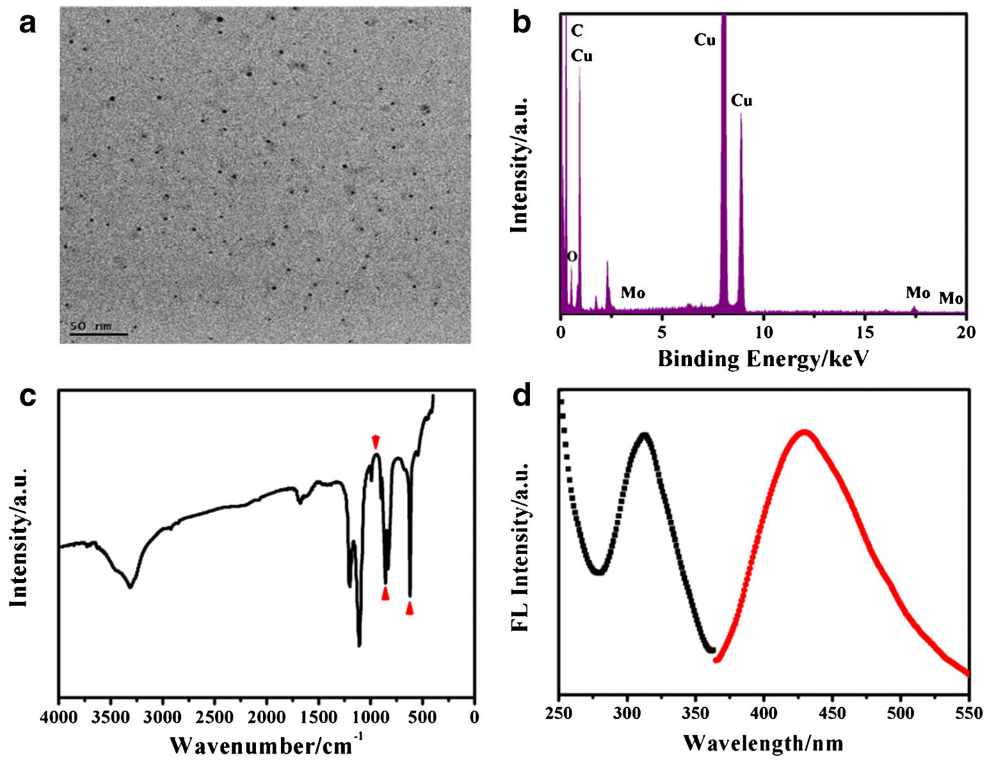

Fig. 1 Representative TEM image (**a**), EDS spectrum (**b**), FT-IR spectrum (**c**), and photoluminescence excitation and emission spectra (**d**) of MoO_x QDs

ECL efficiency (Φ_{ECL}) is defined as the number of photons emitted per unit charge transferred during the chemiluminescence reaction and depends on the efficiency of excited state population and the quantum yield of emission from this state. The Φ_{ECL} of MoO_x QDs in solution was calculated using $[Ru(bpy)_3]^{2+}$ as a standard according to the following equation [26].

$$\Phi_{ECL} = \Phi^{\circ}_{ECL}\left(I Q^{\circ}_{f} / Q_{f} I^{\circ}\right) \quad (5)$$

Here, $\Phi^{\circ}_{ECL} = 5.0\%$ is the ECL efficiency of $[Ru(bpy)_3]^{2+}$ obtained via an annihilation mechanism in 0.1 M ACN with 1 mM $(TBA)BF_4$ [27], Q_f and Q°_f are the transferred faradaic charges for the MoO_x QD film and $[Ru(bpy)_3]^{2+}$, respectively, and I and I^{o} are the respective integrated PMT responses. We estimated Φ_{ECL} of MoO_x QDs as 4.23%, revealing the excellent ECL properties of these QDs.

Characterization of the immunosensor

The operation of the ECL immunosensor relies on the specificity of antigen-antibody recognition. MoO_x QDs/Au NPs-chit were used as antibody carriers and sensing platform for GCE modification, and the formation of a non-conductive

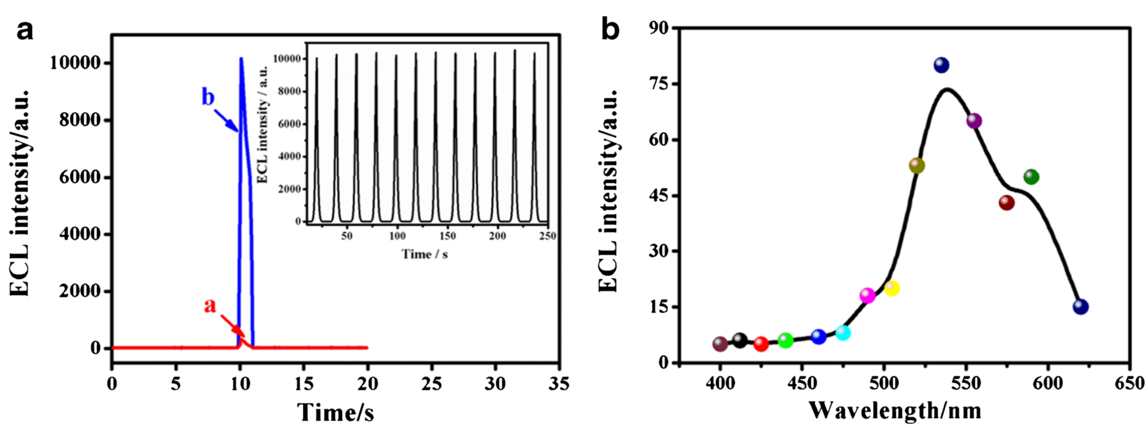

Fig. 2 **a** ECL responses of (a) bare and (b) MoO_x QD-modified GCE in 0.1 M phosphate buffer (pH 5.0) containing 0.1 M $K_2S_2O_8$ and 0.1 M KCl. Inset shows the ECL emission of MoO_x QDs/GCE during 12 continuous voltammetric cycles. **b** ECL spectrum of the MoO_x QDs/$S_2O_8^{2-}$ ECL system

antigen-antibody complex was expected to hinder electron transfer and thus decrease ECL response. The ECL behavior of the immunosensor was investigated in 0.1 M PBS (pH 7.4) containing of 0.1 M KCl and 0.1 M $K_2S_2O_8$ using CYFRA21-1 as a model analyte. As shown in Fig. 3a, MoO_x QDs/GCE exhibits strong ECL emission (curve a), which slightly decreases upon the introduction of Au NPs-chit (curve b). This decrease is attributed to the presence of CS (that is not conducive to ECL) or resonance energy transfer between Au NPs and MoO_x QDs. The introduction of anti-CYFRA21-1 (curve c) and BSA (curve d) results in a further decrease of ECL signal intensity due to the blockage of electron transfer by inert protein molecules. Finally, the immunoreaction of CYFRA21-1 with the immobilized anti-CYFRA21-1 to afford a non-conductive immunocomplex results in an additional intensity decrease (curve e), as this complex hinders electron and mass transfer between ECL reagents and the electrode surface. This suggests that the intensity decrease can be utilized to quantify CYFRA21-1.

To better understand the process of immunosensor fabrication, individual fabrication stages were investigated by cyclic voltammetry (CV) and EIS measurements, which were performed in 5.0 mM $K_3[Fe(CN)_6]/K_4[Fe(CN)_6]$ solution containing 0.10 M KCl. Figure 3b shows the CV curves of the stepwise modified electrode, showing that a pair of well-defined redox peaks (curve a) is observed for the bare GCE. After modification with MoO_x QDs (curve b), the peak current decreases, while peak potential separation (ΔE_p) increases, which suggests that the immobilized MoO_x QDs attenuated electron transfer. However, the subsequent introduction of Au NPs-chit results in an increase of peak current and a decrease of ΔEp (curve c), i.e., the excellent electrical conductivity of Au NPs and the excellent film forming ability and adhesiveness of CS facilitates electron transfer. As the electrode was further incubated with anti-CYFRA21-1, BSA, and CYFRA21-1, the peak current (curves d, e, and f, respectively) progressively decreases, while ΔE_p increases, since the non-conductive protein molecules hinder electron transfer [28, 29]. Figure 3c shows the electrochemical impedance spectra of bare and modified electrodes, demonstrating that the bare GCE (curve a) has a lower impedance than the MoO_x QD-modified GCE (curve b), as MoO_x QDs hinder surface electron transfer. The immobilization of Au NPs-chit results in an obvious decrease of impedance (curve c) due to the excellent electrical conductivity of Au NPs. Finally, the introduction of anti-CYFRA21-1, BSA, and CYFRA21-1 successively increases electron transfer resistance (curves d, e, and f, respectively), as the non-conductive protein layer acts a barrier for electron transfer. Taken together, the above findings are indicative of successful immunosensor fabrication.

Performance of the immunoassay

The immunosensor was used for CYFRA21-1 detection under optimized conditions (Fig. 4). Figure 4a shows that the ECL response (I_{ECL}) decreases with increasing CYFRA21-1 concentration, while Fig. 4b reveals that this decrease linearly depends on the logarithm of CYFRA21-1 concentration (log *c*) within the range of 0.001–350 ng mL^{-1}. The linear relation can be described by the equation $I_{ECL} = 759.5 \log c + 2520$, with a correlation coefficient of 0.9890. The detection limit (0.3 pg mL^{-1}) was calculated as three times the standard deviation of the blank signal. Compared with the previous reports for detection of CYFRA21-1 [30–34], the constructed label-free ECL immunosensor has a good performance in terms of a wider linear range and a lower limit of detection (Table 1).

The operational stability of our sensing platform was investigated under the conditions of continuous cyclic potential scanning (Fig. 4c, 12 cycles at 1 pg mL^{-1} CYFRA21-1 standard solutions) in 0.1 M phosphate buffer (pH 7.4) containing 0.1 M KCl and 0.1 M $K_2S_2O_8$, strong and stable ECL signals are observed (relative standard deviation (RSD) = 0.54%).

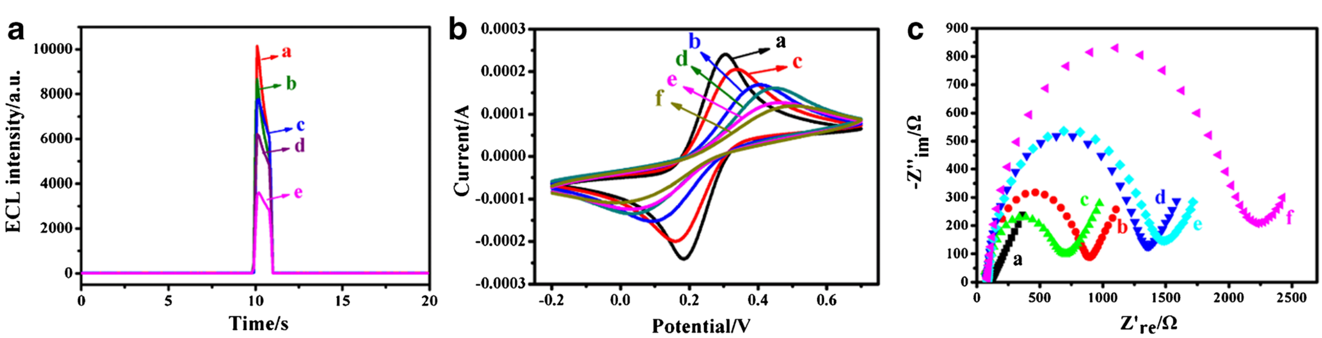

Fig. 3 **a** ECL responses of (a) MoO_x QDs, (b) MoO_x QDs/Au NPs-chit, (c) MoO_x QDs/Au NPs-chit/Ab, (d) MoO_x QDs/Au NPs-chit/Ab/BSA, and (e) MoO_x QDs /Au NPs-chit/Ab/BSA/CYFRA21-1. **b** Cyclic voltammograms and (C) EIS spectra of working electrodes modified with (a) nothing (bare electrode), (b) MoO_x QDs, (c) MoO_x QDs/Au NPs-chit, (d) MoO_x QDs/Au NPs-chit/Ab, (e) MoO_x QDs/Au NPs-chit/BSA/Ab, and (f) MoO_x QDs/Au NPs-chit/BSA/Ab/CYFRA21-1

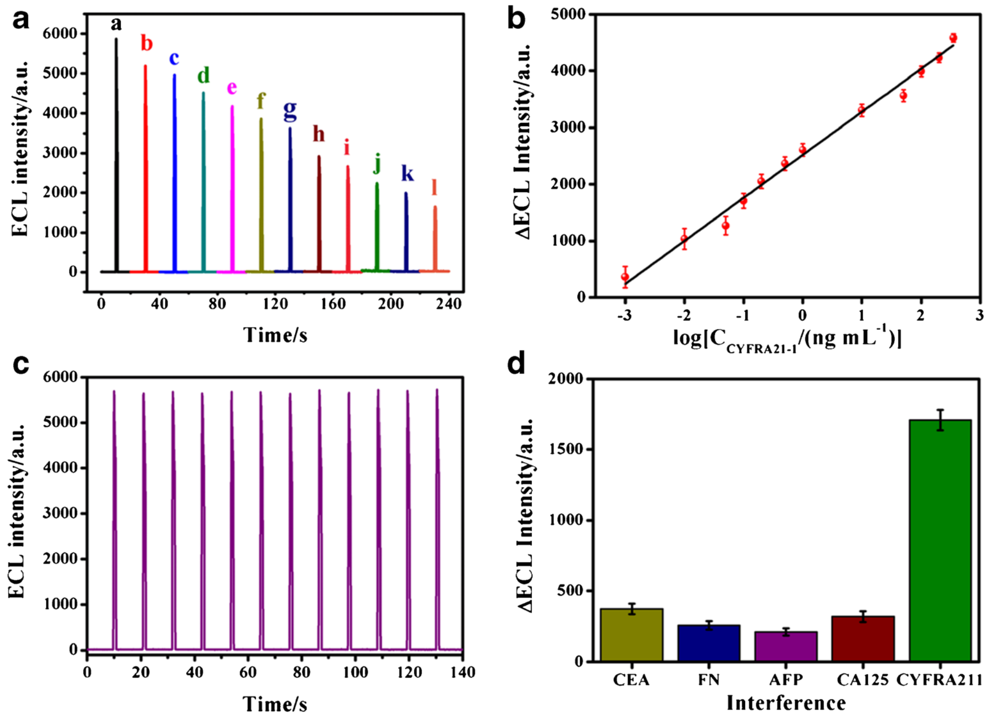

Fig. 4 **a** ECL responses of the immunosensor in 0.1 M phosphate buffer (pH 7.4) containing 0.1 M KCl and 0.1 M $K_2S_2O_8$ to CYFRA21-1 (from a to l: 0.001, 0.01, 0.05, 0.1, 0.2, 0.5, 1, 10, 50, 100, 200, 350 ng mL^{-1}). **b** Dependence of ECL intensity on the concentration of CYFRA21-1. **c** Stability of ECL emission from GCE/MoO_x QDs/Au NPs-chit/Ab/BSA under continuous scanning for 12 cycles at 1 pg mL^{-1} CYFRA21-1 in 0.1 M phosphate buffer (pH 7.4) containing 0.1 M KCl and 0.1 M $K_2S_2O_8$. **d** Responses of the fabricated ECL sensor to different proteins. ΔECL intensity I_0-I, where I_0 and I are the ECL intensities of GCE/MoOx QDs/Au NPs-chit/Ab/BSA in $K_2S_2O_8$ solution in the absence and presence of targets, respectively

Furthermore, we demonstrates that >90% of ECL intensity is retained after four-week storage at 4 °C and thus shows that the fabricated immunosensor exhibits excellent stability. Finally, sensor reproducibility was examined by determining intra- and inter-assay precisions. The former parameter was estimated by measuring the response of the sensor to 1 pg mL^{-1} CYFRA21-1 for six times, while the latter was determined by assaying the response of 10 modified electrodes to 1 pg mL^{-1} CYFRA21-1. As a result, intra- and inter-assay RSDs were obtained as 3.18 and 4.39%, respectively, which indicates that the fabricated immunosensor provides well-reproducible results. Besides, after the antigen of CYFRA21-1 was incubated onto the GCE/MoO_x QDs/Au NPs-chit/BSA/Ab for 1 h, the electrode surface was regenerated by treatment with Gly − HCl (pH 2.2) buffer containing 0.05% Tween 20 to remove the coupled CYFRA21-1 on the electrode surface [35]. After each acid treatment, the surface was again incubated with the CYFRA21-1. The results displays that the immunosensor is stable up to 7 recycles without obvious loss of affinity and residual of CYFRA21-1 after elusion.

To further investigate the specificity of our immunosensor, we examined its responses to several interfering proteins, namely CEA, FN, AFP, and CA125 (Fig. 4d). Notably, responses to these proteins (0.2 μg mL^{-1}) are much weaker than that to a 2000-fold smaller concentration of CYFRA21-1 (0.1 ng mL^{-1}), which demonstrates the excellent specificity of our sensor.

Table 1 Comparisons of different method for CYFRA21-1 detection

Detection method	Electrode Materials	Linear range (ng mL^{-1})	LOD (pg mL^{-1})	Ref
Electrochemical immunoassay	HAATM/CYFRA21–1/Ab1/GA/3D–G/GCE	0.1–150	43	[30]
Amperometric immunosensor	ZIF–8–HQ–BSA–Ab_2–CYFRA21–1–anti–CYFRA21–1/AuNPs/PANI hydrogel/GCE	1×10^{-4} – 100	0.65	[31]
Electrochemical immunosensor	CYFRA21–1/BSA/Ab1/GA/3D–G @Au/GCE	0.25–800	100	[32]
Electrochemical immunosensor	BSA/anti-CYFRA–21–1/APTES/ZrO_2–RGO/ITO	2–22	122	[33]
Electrochemical immunoassay	PMCP–Au–anti–Cyfra21–1/Cyfra21–1/BSA/anti-Cyfra21–1/GCE	1–150	400	[34]
ECL immunoassay	GCE/MoO_x QDs/Au NPs–chit/BSA/Ab/CYFRA21–1	1.0×10^{-3} – 350	0.3	This work

Real sample application

To test the analytical reliability and application potential of the immunosensor, we employed it for the standard addition method-based analysis of human serum samples spiked with CYFRA21-1 standard solution to different final concentrations (2.00, 5.00, and 10.00 ng mL^{-1}). The human serum samples were collected from the Second Hospital of Fuzhou. Prior to measurement, the serum samples were diluted 10 times (1:10 diluted with 0.1 M phosphate buffer solution, pH 7.4). Following that, 5 μL of the above sample was dropped onto the immunosensor and then thoroughly washed with phosphate buffer (0.1 M, pH 7.4) after the immunoreaction with 30 min of incubation at 37 °C. The concentration of CYFRA21-1 in the serum sample was calculated according to its degree of ECL inhibition. With the addition of different concentrations of CYFRA21-1 standard into the serum sample, the recoveries were calculated. As shown in Table 2, the observed recoveries range from 98.6 to 103.1%, while the corresponding RSDs range from 4.53 to 7.21%, which indicated that the resulting sensor has potential application in complicated real samples.

Conclusions

An ECL sensing platform based on MoO_x QDs/Au NPs-chitosan film has been successfully fabricated. MoO_x QDs were used as the ECL probe due to their excellent ECL performance with $K_2S_2O_8$ as co-reactant. Under the optimized experimental conditions, CYFRA21-1 can be effectively assayed by monitoring the decreased ECL response upon the immunoreaction on the sensor surface. The immunoassay displays good performances with a wide linear range, high sensitivity, acceptable stability and reproducibility, indicating its potential applications for the detection of other biomolecules, such as other biomarkers, DNA, and cell. However, the relatively complex preparation process and low detection potential applied in this system might cause some side reactions for real samples detection, which limiting the application of MoO_x QDs in other ECL sensors.

Table 2 Recovery results of CYFRA 21-1 at different concentrations spiked into human serum samples

Sample	Added (ng mL^{-1})	Found (ng mL^{-1})	Recovery (%)
1	0	6.60 ± 0.36	–
	2.00	8.87 ± 0.55	103.1
2	0	6.33 ± 0.39	–
	5.00	11.17 ± 0.71	98.6
3	0	7.16 ± 0.53	–
	10.00	17.62 ± 1.62	102.7

Acknowledgments We sincerely acknowledge the financial support of the National Natural Science Foundation of China (21874020, 21405015), Fujian Province Health Commission Young and Middle-Aged Talent training project (2018-ZQN-62), Fujian Province Young Talent Supporting Project (2019B016), Joint Funds for the Innovation of Science and Technology, Fujian Province (2016Y9056, 2016Y9054), the Science and Technology Project of Fujian Province (2018 L3008), the Natural Science Foundation of Shandong Province (ZR2016BL19), and Program for Fujian Top-notch Innovative Personnel.

Compliance with ethical standards

Conflict of interest The author(s) declare that they have no competing interests.

References

1. Lv XH, Pang XH, Li YY, Yan T, Cao W, Du B, Wei Q (2015) Electrochemiluminescent immune-modified electrodes based on Ag_2Se@CdSe Nanoneedles loaded with Polypyrrole intercalated Graphene for detection of CA72-4. ACS Appl Mater Interfaces 7: 867–872
2. Yao X, Yan PP, Tang QH, Deng AP, Li JG (2013) Quantum dots based electrochemiluminescent immunosensor by coupling enzymatic amplification for ultrasensitive detection of clenbuterol. Anal Chim Acta 798:82–88
3. Yan PP, Zhang J, Tang QH, Deng AP, Li JG (2014) A quantum dot based electrochemiluminescent immunosensor for the detection of pg level phenylethanolamine a using gold nanoparticles as substrates and electron transfer accelerators. Analyst 139:4365–4372
4. Liu X, Jiang H, Fang Y, Zhao W, Wang NY, Zang GZ (2015) Quantum dots based potential-resolution dual-targets Electrochemiluminescent Immunosensor for subtype of tumor marker and its serological evaluation. Anal Chem 87:9163–9169
5. Pang XH, Li JX, Zhao YB, Wu D, Zhang Y, Du B, Ma HM, Wei Q (2015) Label-free Electrochemiluminescent Immunosensor for detection of Carcinoembryonic antigen based on Nanocomposites of GO/MWCNTs-COOH/au@CeO_2. ACS Appl Mater Interfaces 7: 19260–19267
6. Geng J, Jia XD, Zhu JJ (2011) Sonochemical selective synthesis of ZnO/CdS core/shell nanostructures and their optical properties. CrystEngComm 13:193–198
7. Zhou J, Han TQ, Ma HM, Yan T, Pang XH, Li YY, Wei Q (2015) A novel electrochemiluminescent immunosensor based on the quenching effect of aminated graphene on nitrogen-doped carbon quantum dots. Anal Chim Acta 889:82–89
8. Hu LY, Zheng J, Zhao K, Deng AP, Li JG (2018) An ultrasensitive electrochemiluminescent immunosensor based on graphene oxide coupled graphite-like carbon nitride and multiwalled carbon nanotubes-gold for the detection of diclofenac. Biosens Bioelectron 101:260–267
9. Peng HP, Jian ML, Deng HH, Wang WJ, Huang ZN, Huang KY, Liu AL, Chen W (2017) Valence states effect on Electrogenerated Chemiluminescence of gold Nanocluster. ACS Appl Mater Interfaces 9:14929–14934
10. Zhang L, Hong MF, Chu ZJ, Xu H, Wang SP, Zhao XJ, Xiao SJ (2018) A new copper mediated on-off assay for alkaline phosphatase detection based on MoOx quantum dots. Microchem J 141: 170–175
11. Xiao SJ, Zhao XJ, Zuo J, Huang HQ, Zhang L (2016) Highly photoluminescent MoO_x quantum dots: facile synthesis and application in off-on pi sensing in lake water samples. Anal Chim Acta 906:148–155

12. Xiao SJ, Chu ZJ, Zhao XJ, Zhang ZB, Liu YH (2017) Off-on-off detection of the activity of acetylcholine esterase and its inhibitors using MoO_x quantum dots as a photoluminescent probe. Microchim Acta 184:4853–4860
13. Yuan LL, Niu YS, Li RG, Zheng LH, Wang Y, Liu ML, Xu GF, Huang L, Xu YH (2018) Molybdenum oxide quantum dots prepared via a one-step stirring strategy and their application as fluorescent probes for pyrophosphate sensing and efficient antibacterial materials. J Mater Chem B 6:3240–3245
14. Wang N, Tang DY, Zou HY, Jia SY, Sun ZJ, Yang X, Peng J (2018) Synthesis of molybdenum oxide quantum dots with better dispersity and bio-imaging ability by reduction method. Opt Mater 83:19–27
15. Xiao SJ, Zhao XJ, Hu PP, Chu ZJ, Huang CZ, Zhang L (2016) Highly Photoluminescent molybdenum oxide quantum dots: one-pot synthesis and application in 2,4,6-trinitrotoluene determination. ACS Appl Mater Interfaces 8:8184–8191
16. Ding DD, Guo W, Guo CS, Sun JZ, Zheng NN, Wang F, Yan M, Liu SQ (2017) MoO_{3-x} quantum dots for photoacoustic imaging guided photothermal/photodynamic cancer treatment. Nanoscale 9:2020–2029
17. Ding DD, Huang WC, Song CQ, Yan M, Guo CS, Liu SQ (2017) Non-stoichiometric MoO_{3-x} quantum dots as a light-harvesting material for interfacial water evaporation. Chem Commun 53:6744–6747
18. Qiu JD, Peng HZ, Liang RP, Li J, Xia XH (2007) Synthesis, characterization, and immobilization of Prussian blue-modified au nanoparticles: application to Electrocatalytic reduction of H_2O_2. Langmuir 23:2133–2137
19. Sui LL, Xu YM, Zhang XF, Cheng XL, Gao S, Zhao H, Cai Z, Huo LH (2015) Construction of three-dimensional flower-like α-MoO3 with hierarchical structure for highly selective triethylamine sensor. Sensors Actuators B Chem 208:406–414
20. Peng HP, Deng HH, Jian ML, Liu AL, Bai FQ, Lin XH, Chen W (2017) Electrochemiluminescence sensor based on methionine-modified gold nanoclusters for highly sensitive determination of dopamine released by cells. Microchim Acta 184:735–743
21. Ding Z, Quinn BM, Haram SK, Pell LE, Korgel BA, Bard AJ (2002) Electrochemistry and electrogenerated chemiluminescence from silicon nanocrystal quantum dots. Science 296:1293–1297
22. Myung N, Ding Z, Bard AJ (2002) Electrogenerated Chemiluminescence of CdSe Nanocrystals. Nano Lett 2:1315–1319
23. Zhang XL, Tang ZR, Dong YP, Wang CM (2018) Electrogenerated chemiluminescence of ZnO nanorods and its sensitive detection of cytochrome C. Talanta 179:139–144
24. Wu D, Liu Y, Wang Y, Hu L, Ma H, Wang G, Wei Q (2016) Label-free Electrochemiluminescent Immunosensor for detection of prostate specific antigen based on Aminated Graphene quantum dots and carboxyl Graphene quantum dots. Sci Rep 6:20511
25. Lu Q, Wei W, Zhou ZX, Zhou ZX, Zhang YJ, Liu SQ (2014) Electrochemiluminescence resonance energy transfer between graphene quantum dots and gold nanoparticles for DNA damage detection. Analyst 139:2404–2410
26. Dennany L, Hogan CF, Keyes TE, Forster RJ (2006) Effect of surface immobilization on the Electrochemiluminescence of ruthenium-containing Metallopolymers. Anal Chem 78:1412–1417
27. Van Houten J, Watts RJ (1976) Temperature dependence of the photophysical and photochemical properties of the tris(2,2′-bipyridyl)ruthenium(II) ion in aqueous solution. J Am Chem Soc 98:4853–4858
28. Tang M, Zhou ZX, Li SG, Zhao F, Liu SQ (2018) Electrochemiluminescent detection of cardiac troponin I by using soybean peroxidase labeled-antibody as signal amplifier. Talanta 180:47–53
29. Zhou Y, Zhuo Y, Liao N, Chai YQ, Yuan R (2014) Ultrasensitive immunoassay based on a pseudobienzyme amplifying system of choline oxidase and luminol-reduced Pt@au hybrid nanoflowers. Chem Commun 50:14627–14630
30. Zeng Y, Bao J, Zhao YN, Huo DQ, Chen M, Qi YL, Yang M, Fa HB, Hou CJ (2018) A sandwich-type electrochemical immunoassay for ultrasensitive detection of non-small cell lung cancer biomarker CYFRA21-1. Bioelectrochemistry 120:183–189
31. Wang HQ, Ma ZF (2019) “Off-on” signal amplification strategy amperometric immunosensor for ultrasensitive detection of tumour marker. Biosens Bioelectron 132:265–270
32. Zeng Y, Bao J, Zhao YN, Huo DQ, Chen M, Yang M, Fa HB, Hou CJ (2018) A sensitive label-free electrochemical immunosensor for detection of cytokeratin 19 fragment antigen 21-1 based on 3D graphene with gold nanopaticle modified electrode. Talanta 178:122–128
33. Kumar S, Sharma JG, Maji S, Malhotra BD (2016) Nanostructured zirconia decorated reduced graphene oxide based efficient biosensing platform for non-invasive oral cancer detection. Biosens Bioelectron 78:497–504
34. Shan J, Ma ZF (2016) Simultaneous detection of five biomarkers of lung cancer by electrochemical immunoassay. Microchim Acta 183:2889–2897
35. Han L, Wang D, Yan L, Petrenko VA, Liu AH (2019) Specific phages-based electrochemical impedimetric immunosensors for label-free and ultrasensitive detection of dual prostate-specific antigens. Sensors Actuators B Chem 297:126727